Observation of Three Charmonium-like States with $J^{PC} = 1^{--}$ in $e^+e^- \to D^{*0}D^{*-}\pi^+ + c.c.$ Process

M. Ablikim[1], M. N. Achasov[13,b], P. Adlarson[73], R. Aliberti[34], A. Amoroso[72A,72C], M. R. An[38], Q. An[69,56], Y. Bai[55], O. Bakina[35], I. Balossino[29A], Y. Ban[45,g], V. Batozskaya[1,43], K. Begzsuren[31], N. Berger[34], M. Bertani[28A], D. Bettoni[29A], F. Bianchi[72A,72C], E. Bianco[72A,72C], J. Bloms[66], A. Bortone[72A,72C], I. Boyko[35], R. A. Briere[5], A. Brueggemann[66], H. Cai[74], X. Cai[1,56], A. Calcaterra[28A], G. F. Cao[1,61], N. Cao[1,61], S. A. Cetin[60A], J. F. Chang[1,56], T. T. Chang[75], W. L. Chang[1,61], G. R. Che[42], G. Chelkov[35,a], C. Chen[42], Chao Chen[53], G. Chen[1], H. S. Chen[1,61], M. L. Chen[1,56,61], S. J. Chen[41], S. M. Chen[59], T. Chen[1,61], X. R. Chen[30,61], X. T. Chen[1,61], Y. B. Chen[1,56], Y. Q. Chen[33], Z. J. Chen[25,h], W. S. Cheng[72C], S. K. Choi[10A], X. Chu[42], G. Cibinetto[29A], S. C. Coen[4], F. Cossio[72C], J. J. Cui[48], H. L. Dai[1,56], J. P. Dai[77], A. Dbeyssi[19], R. E. de Boer[4], D. Dedovich[35], Z. Y. Deng[1], A. Denig[34], I. Denysenko[35], M. Destefanis[72A,72C], F. De Mori[72A,72C], B. Ding[64,1], X. X. Ding[45,g], Y. Ding[39], Y. Ding[33], J. Dong[1,56], L. Y. Dong[1,61], M. Y. Dong[1,56,61], X. Dong[74], S. X. Du[79], Z. H. Duan[41], P. Egorov[35,a], Y. L. Fan[74], J. Fang[1,56], S. S. Fang[1,61], W. X. Fang[1], Y. Fang[1], R. Farinelli[29A], L. Fava[72B,72C], F. Feldbauer[4], G. Felici[28A], C. Q. Feng[69,56], J. H. Feng[57], K Fischer[67], M. Fritsch[4], C. Fritzsch[66], C. D. Fu[1], Y. W. Fu[1], H. Gao[61], Y. N. Gao[45,g], Yang Gao[69,56], S. Garbolino[72C], I. Garzia[29A,29B], P. T. Ge[74], Z. W. Ge[41], C. Geng[57], E. M. Gersabeck[65], A Gilman[67], K. Goetzen[14], L. Gong[39], W. X. Gong[1,56], W. Gradl[34], S. Gramigna[29A,29B], M. Greco[72A,72C], M. H. Gu[1,56], Y. T. Gu[16], C. Y Guan[1,61], Z. L. Guan[22], A. Q. Guo[30,61], L. B. Guo[40], R. P. Guo[47], Y. P. Guo[12,f], A. Guskov[35,a], X. T. H.[1,61], W. Y. Han[38], X. Q. Hao[20], F. A. Harris[63], K. K. He[53], K. L. He[1,61], F. H. Heinsius[4], C. H. Heinz[34], Y. K. Heng[1,56,61], C. Herold[58], T. Holtmann[4], P. C. Hong[12,f], G. Y. Hou[1,61], Y. R. Hou[61], Z. L. Hou[1], H. M. Hu[1,61], J. F. Hu[54,i], T. Hu[1,56,61], Y. Hu[1], G. S. Huang[69,56], K. X. Huang[57], L. Q. Huang[30,61], X. T. Huang[48], Y. P. Huang[1], T. Hussain[71], N Hüsken[27,34], W. Imoehl[27], M. Irshad[69,56], J. Jackson[27], S. Jaeger[4], S. Janchiv[31], J. H. Jeong[10A], Q. Ji[1], Q. P. Ji[20], X. B. Ji[1,61], X. L. Ji[1,56], Y. Y. Ji[48], Z. K. Jia[69,56], P. C. Jiang[45,g], S. S. Jiang[38], T. J. Jiang[17], X. S. Jiang[1,56,61], Y. Jiang[61], J. B. Jiao[48], Z. Jiao[23], S. Jin[41], Y. Jin[64], M. Q. Jing[1,61], T. Johansson[73], X. K.[1], S. Kabana[32], N. Kalantar-Nayestanaki[62], X. L. Kang[9], X. S. Kang[39], R. Kappert[62], M. Kavatsyuk[62], B. C. Ke[79], A. Khoukaz[66], R. Kiuchi[1], R. Kliemt[14], L. Koch[36], O. B. Kolcu[60A], B. Kopf[4], M. Kuessner[4], A. Kupsc[43,73], W. Kühn[36], J. J. Lane[65], J. S. Lange[36], P. Larin[19], A. Lavania[26], L. Lavezzi[72A,72C], T. T. Lei[69,k], Z. H. Lei[69,56], H. Leithoff[34], M. Lellmann[34], T. Lenz[34], C. Li[46], C. Li[42], C. H. Li[38], Cheng Li[69,56], D. M. Li[79], F. Li[1,56], G. Li[1], H. Li[69,56], H. B. Li[1,61], H. J. Li[20], H. N. Li[54,i], Hui Li[42], J. R. Li[59], J. S. Li[57], J. W. Li[48], Ke Li[1], L. J Li[1,61], L. K. Li[1], Lei Li[3], M. H. Li[42], P. R. Li[37,j,k], S. X. Li[12], T. Li[48], W. D. Li[1,61], W. G. Li[1], X. H. Li[69,56], X. L. Li[48], Xiaoyu Li[1,61], Y. G. Li[45,g], Z. J. Li[57], Z. X. Li[16], Z. Y. Li[57], C. Liang[41], H. Liang[69,56], H. Liang[33], H. Liang[1,61], Y. F. Liang[52], Y. T. Liang[30,61], G. R. Liao[15], L. Z. Liao[48], J. Libby[26], A. Limphirat[58], D. X. Lin[30,61], T. Lin[1], B. X. Liu[74], B. J. Liu[1], C. Liu[33], C. X. Liu[1], D. Liu[19,69], F. H. Liu[51], Fang Liu[1], Feng Liu[6], G. M. Liu[54,i], H. Liu[37,j,k], H. B. Liu[16], H. M. Liu[1,61], Huanhuan Liu[1], Huihui Liu[21], J. B. Liu[69,56], J. L. Liu[70], J. Y. Liu[1,61], K. Liu[1], K. Y. Liu[39], Ke Liu[22], L. Liu[69,56], L. C. Liu[42], Lu Liu[42], M. H. Liu[12,f], P. L. Liu[1], Q. Liu[61], S. B. Liu[69,56], T. Liu[12,f], W. K. Liu[42], W. M. Liu[69,56], X. Liu[37,j,k], Y. Liu[37,j,k], Y. B. Liu[42], Z. A. Liu[1,56,61], Z. Q. Liu[48], X. C. Lou[1,56,61], F. X. Lu[57], H. J. Lu[23], J. G. Lu[1,56], X. L. Lu[1], Y. Lu[7], Y. P. Lu[1,56], Z. H. Lu[1,61], C. L. Luo[40], M. X. Luo[78], T. Luo[12,f], X. L. Luo[1,56], X. R. Lyu[61], Y. F. Lyu[42], F. C. Ma[39], H. L. Ma[1], J. L. Ma[1,61], L. L. Ma[48], M. M. Ma[1,61], Q. M. Ma[1], R. Q. Ma[1,61], R. T. Ma[61], X. Y. Ma[1,56], Y. Ma[45,g], F. E. Maas[19], M. Maggiora[72A,72C], S. Maldaner[4], S. Malde[67], A. Mangoni[28B], Y. J. Mao[45,g], Z. P. Mao[1], S. Marcello[72A,72C], Z. X. Meng[64], J. G. Messchendorp[14,62], G. Mezzadri[29A], H. Miao[1,61], T. J. Min[41], R. E. Mitchell[27], X. H. Mo[1,56,61], N. Yu. Muchnoi[13,b], Y. Nefedov[35], F. Nerling[19,d], I. B. Nikolaev[13,b], Z. Ning[1,56], S. Nisar[11,l], Y. Niu [48], S. L. Olsen[61], Q. Ouyang[1,56,61], S. Pacetti[28B,28C], X. Pan[53], Y. Pan[55], A. Pathak[33], Y. P. Pei[69,56], M. Pelizaeus[4], H. P. Peng[69,56], K. Peters[14,d], J. L. Ping[40], R. G. Ping[1,61], S. Plura[34], S. Pogodin[35], V. Prasad[32], F. Z. Qi[1], H. Qi[69,56], H. R. Qi[59], M. Qi[41], T. Y. Qi[12,f], S. Qian[1,56], W. B. Qian[61], C. F. Qiao[61], J. J. Qin[70], L. Q. Qin[15], X. P. Qin[12,f], X. S. Qin[48], Z. H. Qin[1,56], J. F. Qiu[1], S. Q. Qu[59], C. F. Redmer[34], K. J. Ren[38], A. Rivetti[72C], V. Rodin[62], M. Rolo[72C], G. Rong[1,61], Ch. Rosner[19], S. N. Ruan[42], N. Salone[43], A. Sarantsev[35,c], Y. Schelhaas[34], K. Schoenning[73], M. Scodeggio[29A,29B], K. Y. Shan[12,f], W. Shan[24], X. Y. Shan[69,56], J. F. Shangguan[53], L. G. Shao[1,61], M. Shao[69,56], C. P. Shen[12,f], H. F. Shen[1,61], W. H. Shen[61], X. Y. Shen[1,61], B. A. Shi[61], H. C. Shi[69,56], J. Y. Shi[1], Q. Q. Shi[53], R. S. Shi[1,61], X. Shi[1,56], J. J. Song[20], T. Z. Song[57], W. M. Song[33,1], Y. X. Song[45,g], S. Sosio[72A,72C], S. Spataro[72A,72C], F. Stieler[34], Y. J. Su[61], G. B. Sun[74], G. X. Sun[1], H. Sun[61], H. K. Sun[1], J. F. Sun[20], K. Sun[59], L. Sun[74], S. S. Sun[1,61], T. Sun[1,61], W. Y. Sun[33], Y. Sun[9], Y. J. Sun[69,56], Y. Z. Sun[1], Z. T. Sun[48], Y. X. Tan[69,56], C. J. Tang[52], G. Y. Tang[1], J. Tang[57], Y. A. Tang[74], L. Y Tao[70], Q. T. Tao[25,h], M. Tat[67], J. X. Teng[69,56], V. Thoren[73], W. H. Tian[57], W. H. Tian[50], Y. Tian[30,61], Z. F. Tian[74], I. Uman[60B], B. Wang[1], B. L. Wang[61], Bo Wang[69,56], C. W. Wang[41], D. Y. Wang[45,g], F. Wang[70], H. J. Wang[37,j,k], H. P. Wang[1,61], K. Wang[1,56], L. L. Wang[1], M. Wang[48], Meng Wang[1,61], S. Wang[12,f], T. Wang[12,f], T. J. Wang[42], W. Wang[57], W. Wang[70], W. H. Wang[74], W. P. Wang[69,56], X. Wang[45,g], X. F. Wang[37,j,k], X. J. Wang[38], X. L. Wang[12,f], Y. Wang[59], Y. D. Wang[44], Y. F. Wang[1,56,61], Y. H. Wang[46], Y. N. Wang[44], Y. Q. Wang[1], Yaqian Wang[18,1], Yi Wang[59], Z. Wang[1,56], Z. L. Wang[70], Z. Y. Wang[1,61], Ziyi Wang[61], D. Wei[68], D. H. Wei[15], F. Weidner[66], S. P. Wen[1], C. W. Wenzel[4], U. Wiedner[4], G. Wilkinson[67], M. Wolke[73], L. Wollenberg[4], C. Wu[38], J. F. Wu[1,61], L. H. Wu[1], L. J. Wu[1,61], X. Wu[12,f], X. H. Wu[33], Y. Wu[69], Y. J Wu[30], Z. Wu[1,56], L. Xia[69,56], X. M. Xian[38], T. Xiang[45,g], D. Xiao[37,j,k], G. Y. Xiao[41], H. Xiao[12,f], S. Y. Xiao[1], Y. L. Xiao[12,f], Z. J. Xiao[40], C. Xie[41], X. H. Xie[45,g], Y. Xie[48], Y. G. Xie[1,56], Y. H. Xie[6], Z. P. Xie[69,56], T. Y. Xing[1,61], C. F. Xu[1,61], C. J. Xu[57], G. F. Xu[1], H. Y. Xu[64], Q. J. Xu[17], W. L. Xu[64], X. P. Xu[53], Y. C. Xu[76], Z. P. Xu[41], Z. S. Xu[61], F. Yan[12,f], L. Yan[12,f], W. B. Yan[69,56], W. C. Yan[79], X. Q Yan[1], H. J. Yang[49,e], H. L. Yang[33], H. X. Yang[1], Tao Yang[1], Y. Yang[12,f], Y. F. Yang[42], Y. X. Yang[1,61], Yifan Yang[1,61], M. Ye[1,56], M. H. Ye[8], J. H. Yin[1], Z. Y. You[57], B. X. Yu[1,56,61], C. X. Yu[42], G. Yu[1,61], T. Yu[70], X. D. Yu[45,g], C. Z. Yuan[1,61], L. Yuan[2], S. C. Yuan[1], X. Q. Yuan[1], Y. Yuan[1,61], Z. Y. Yuan[57], C. X. Yue[38], A. A. Zafar[71], F. R. Zeng[48],

X. Zeng[12,f], Y. Zeng[25,h], Y. J. Zeng[1,61], X. Y. Zhai[33], Y. H. Zhan[57], A. Q. Zhang[1,61], B. L. Zhang[1,61], B. X. Zhang[1], D. H. Zhang[42], G. Y. Zhang[20], H. Zhang[69], H. H. Zhang[33], H. H. Zhang[57], H. Q. Zhang[1,56,61], H. Y. Zhang[1,56], J. J. Zhang[50], J. L. Zhang[75], J. Q. Zhang[40], J. W. Zhang[1,56,61], J. X. Zhang[37,j,k], J. Y. Zhang[1], J. Z. Zhang[1,61], Jiawei Zhang[1,61], L. M. Zhang[59], L. Q. Zhang[57], Lei Zhang[41], P. Zhang[1], Q. Y. Zhang[38,79], Shuihan Zhang[1,61], Shulei Zhang[25,h], X. D. Zhang[44], X. M. Zhang[1], X. Y. Zhang[53], X. Y. Zhang[48], Y. Zhang[67], Y. T. Zhang[79], Y. H. Zhang[1,56], Yan Zhang[69,56], Yao Zhang[1], Z. H. Zhang[1], Z. L. Zhang[33], Z. Y. Zhang[74], Z. Y. Zhang[42], G. Zhao[1], J. Zhao[38], J. Y. Zhao[1,61], J. Z. Zhao[1,56], Lei Zhao[69,56], Ling Zhao[1], M. G. Zhao[42], S. J. Zhao[79], Y. B. Zhao[1,56], Y. X. Zhao[30,61], Z. G. Zhao[69,56], A. Zhemchugov[35,a], B. Zheng[70], J. P. Zheng[1,56], W. J. Zheng[1,61], Y. H. Zheng[61], B. Zhong[40], X. Zhong[57], H. Zhou[48], L. P. Zhou[1,61], X. Zhou[74], X. K. Zhou[6], X. R. Zhou[69,56], X. Y. Zhou[38], Y. Z. Zhou[12,f], J. Zhu[42], K. Zhu[1], K. J. Zhu[1,56,61], L. Zhu[33], L. X. Zhu[61], S. H. Zhu[68], S. Q. Zhu[41], T. J. Zhu[12,f], W. J. Zhu[12,f], Y. C. Zhu[69,56], Z. A. Zhu[1,61], J. H. Zou[1], J. Zu[69,56]

(BESIII Collaboration)

[1] *Institute of High Energy Physics, Beijing 100049, People's Republic of China*
[2] *Beihang University, Beijing 100191, People's Republic of China*
[3] *Beijing Institute of Petrochemical Technology, Beijing 102617, People's Republic of China*
[4] *Bochum Ruhr-University, D-44780 Bochum, Germany*
[5] *Carnegie Mellon University, Pittsburgh, Pennsylvania 15213, USA*
[6] *Central China Normal University, Wuhan 430079, People's Republic of China*
[7] *Central South University, Changsha 410083, People's Republic of China*
[8] *China Center of Advanced Science and Technology, Beijing 100190, People's Republic of China*
[9] *China University of Geosciences, Wuhan 430074, People's Republic of China*
[10] *Chung-Ang University, Seoul, 06974, Republic of Korea*
[11] *COMSATS University Islamabad, Lahore Campus, Defence Road, Off Raiwind Road, 54000 Lahore, Pakistan*
[12] *Fudan University, Shanghai 200433, People's Republic of China*
[13] *G.I. Budker Institute of Nuclear Physics SB RAS (BINP), Novosibirsk 630090, Russia*
[14] *GSI Helmholtzcentre for Heavy Ion Research GmbH, D-64291 Darmstadt, Germany*
[15] *Guangxi Normal University, Guilin 541004, People's Republic of China*
[16] *Guangxi University, Nanning 530004, People's Republic of China*
[17] *Hangzhou Normal University, Hangzhou 310036, People's Republic of China*
[18] *Hebei University, Baoding 071002, People's Republic of China*
[19] *Helmholtz Institute Mainz, Staudinger Weg 18, D-55099 Mainz, Germany*
[20] *Henan Normal University, Xinxiang 453007, People's Republic of China*
[21] *Henan University of Science and Technology, Luoyang 471003, People's Republic of China*
[22] *Henan University of Technology, Zhengzhou 450001, People's Republic of China*
[23] *Huangshan College, Huangshan 245000, People's Republic of China*
[24] *Hunan Normal University, Changsha 410081, People's Republic of China*
[25] *Hunan University, Changsha 410082, People's Republic of China*
[26] *Indian Institute of Technology Madras, Chennai 600036, India*
[27] *Indiana University, Bloomington, Indiana 47405, USA*
[28] *INFN Laboratori Nazionali di Frascati , (A)INFN Laboratori Nazionali di Frascati, I-00044, Frascati, Italy; (B)INFN Sezione di Perugia, I-06100, Perugia, Italy; (C)University of Perugia, I-06100, Perugia, Italy*
[29] *INFN Sezione di Ferrara, (A)INFN Sezione di Ferrara, I-44122, Ferrara, Italy; (B)University of Ferrara, I-44122, Ferrara, Italy*
[30] *Institute of Modern Physics, Lanzhou 730000, People's Republic of China*
[31] *Institute of Physics and Technology, Peace Avenue 54B, Ulaanbaatar 13330, Mongolia*
[32] *Instituto de Alta Investigación, Universidad de Tarapacá, Casilla 7D, Arica, Chile*
[33] *Jilin University, Changchun 130012, People's Republic of China*
[34] *Johannes Gutenberg University of Mainz, Johann-Joachim-Becher-Weg 45, D-55099 Mainz, Germany*
[35] *Joint Institute for Nuclear Research, 141980 Dubna, Moscow region, Russia*
[36] *Justus-Liebig-Universitaet Giessen, II. Physikalisches Institut, Heinrich-Buff-Ring 16, D-35392 Giessen, Germany*
[37] *Lanzhou University, Lanzhou 730000, People's Republic of China*
[38] *Liaoning Normal University, Dalian 116029, People's Republic of China*
[39] *Liaoning University, Shenyang 110036, People's Republic of China*
[40] *Nanjing Normal University, Nanjing 210023, People's Republic of China*
[41] *Nanjing University, Nanjing 210093, People's Republic of China*
[42] *Nankai University, Tianjin 300071, People's Republic of China*
[43] *National Centre for Nuclear Research, Warsaw 02-093, Poland*
[44] *North China Electric Power University, Beijing 102206, People's Republic of China*
[45] *Peking University, Beijing 100871, People's Republic of China*
[46] *Qufu Normal University, Qufu 273165, People's Republic of China*
[47] *Shandong Normal University, Jinan 250014, People's Republic of China*
[48] *Shandong University, Jinan 250100, People's Republic of China*
[49] *Shanghai Jiao Tong University, Shanghai 200240, People's Republic of China*

[50] Shanxi Normal University, Linfen 041004, People's Republic of China
[51] Shanxi University, Taiyuan 030006, People's Republic of China
[52] Sichuan University, Chengdu 610064, People's Republic of China
[53] Soochow University, Suzhou 215006, People's Republic of China
[54] South China Normal University, Guangzhou 510006, People's Republic of China
[55] Southeast University, Nanjing 211100, People's Republic of China
[56] State Key Laboratory of Particle Detection and Electronics, Beijing 100049, Hefei 230026, People's Republic of China
[57] Sun Yat-Sen University, Guangzhou 510275, People's Republic of China
[58] Suranaree University of Technology, University Avenue 111, Nakhon Ratchasima 30000, Thailand
[59] Tsinghua University, Beijing 100084, People's Republic of China
[60] Turkish Accelerator Center Particle Factory Group, (A)Istinye University, 34010, Istanbul, Turkey; (B)Near East University, Nicosia, North Cyprus, 99138, Mersin 10, Turkey
[61] University of Chinese Academy of Sciences, Beijing 100049, People's Republic of China
[62] University of Groningen, NL-9747 AA Groningen, The Netherlands
[63] University of Hawaii, Honolulu, Hawaii 96822, USA
[64] University of Jinan, Jinan 250022, People's Republic of China
[65] University of Manchester, Oxford Road, Manchester, M13 9PL, United Kingdom
[66] University of Muenster, Wilhelm-Klemm-Strasse 9, 48149 Muenster, Germany
[67] University of Oxford, Keble Road, Oxford OX13RH, United Kingdom
[68] University of Science and Technology Liaoning, Anshan 114051, People's Republic of China
[69] University of Science and Technology of China, Hefei 230026, People's Republic of China
[70] University of South China, Hengyang 421001, People's Republic of China
[71] University of the Punjab, Lahore-54590, Pakistan
[72] University of Turin and INFN, (A)University of Turin, I-10125, Turin, Italy; (B)University of Eastern Piedmont, I-15121, Alessandria, Italy; (C)INFN, I-10125, Turin, Italy
[73] Uppsala University, Box 516, SE-75120 Uppsala, Sweden
[74] Wuhan University, Wuhan 430072, People's Republic of China
[75] Xinyang Normal University, Xinyang 464000, People's Republic of China
[76] Yantai University, Yantai 264005, People's Republic of China
[77] Yunnan University, Kunming 650500, People's Republic of China
[78] Zhejiang University, Hangzhou 310027, People's Republic of China
[79] Zhengzhou University, Zhengzhou 450001, People's Republic of China

[a] Also at the Moscow Institute of Physics and Technology, Moscow 141700, Russia
[b] Also at the Novosibirsk State University, Novosibirsk, 630090, Russia
[c] Also at the NRC "Kurchatov Institute", PNPI, 188300, Gatchina, Russia
[d] Also at Goethe University Frankfurt, 60323 Frankfurt am Main, Germany
[e] Also at Key Laboratory for Particle Physics, Astrophysics and Cosmology, Ministry of Education; Shanghai Key Laboratory for Particle Physics and Cosmology; Institute of Nuclear and Particle Physics, Shanghai 200240, People's Republic of China
[f] Also at Key Laboratory of Nuclear Physics and Ion-beam Application (MOE) and Institute of Modern Physics, Fudan University, Shanghai 200443, People's Republic of China
[g] Also at State Key Laboratory of Nuclear Physics and Technology, Peking University, Beijing 100871, People's Republic of China
[h] Also at School of Physics and Electronics, Hunan University, Changsha 410082, China
[i] Also at Guangdong Provincial Key Laboratory of Nuclear Science, Institute of Quantum Matter, South China Normal University, Guangzhou 510006, China
[j] Also at Frontiers Science Center for Rare Isotopes, Lanzhou University, Lanzhou 730000, People's Republic of China
[k] Also at Lanzhou Center for Theoretical Physics, Lanzhou University, Lanzhou 730000, People's Republic of China
[l] Also at the Department of Mathematical Sciences, IBA, Karachi , Pakistan
(Dated: **January 19, 2023)**

The Born cross sections of the process $e^+e^- \to D^{*0}D^{*-}\pi^+ + c.c.$ at center-of-mass energies from 4.189 to 4.951 GeV are measured for the first time. The data samples used correspond to an integrated luminosity of $17.9\,\mathrm{fb}^{-1}$ and were collected by the BESIII detector operating at the BEPCII storage ring. Three enhancements around 4.20, 4.47 and 4.67 GeV are visible. The resonances have masses of $4209.6 \pm 4.7 \pm 5.9\,\mathrm{MeV}/c^2$, $4469.1 \pm 26.2 \pm 3.6\,\mathrm{MeV}/c^2$ and $4675.3 \pm 29.5 \pm 3.5\,\mathrm{MeV}/c^2$ and widths of $81.6 \pm 17.8 \pm 9.0$ MeV, $246.3 \pm 36.7 \pm 9.4$ MeV and $218.3 \pm 72.9 \pm 9.3$ MeV, respectively, where the first uncertainties are statistical and the second systematic. The first and third resonances are consistent with the $Y(4230)$ and $Y(4660)$ states, respectively, while the second one is compatible with the $Y(4500)$ observed in the $e^+e^- \to K^+K^-J/\psi$ process. These three Y states are observed in $e^+e^- \to D^{*0}D^{*-}\pi^+ + c.c.$ process for the first time.

Over the past years, a series of charmonium-like vector meson states with $J^{PC} = 1^{--}$, referred to as Y states, have been observed via electron-positron annihilation in numerous experiments [1]. Dedicated studies of Y states were initially triggered by the discovery of the $Y(4230)$, previously called the $Y(4260)$, in the $e^+e^- \to \pi^+\pi^- J/\psi$ process at BaBar [2], which was confirmed at CLEO [3], Belle [4] and BESIII [5–7]. Later, the $Y(4360)$ and $Y(4660)$ states were established in $e^+e^- \to \pi^+\pi^-\psi(2S)$ at BaBar [8, 9], Belle [10, 11] and BESIII [12–14]. Some similar resonance enhancements around 4.23 GeV, 4.36 GeV or 4.66 GeV are also reported in $\pi^+\pi^- h_c$ [15], $\omega\chi_{c0}$ [16, 17], $\eta J/\psi$ [18], $\eta' J/\psi$ [19], $D^0 D^{*-}\pi^+$ [20], $\pi\pi\psi_2(3823)$ [21], $\pi^+\pi^- D^+ D^-$ [22, 23] and $K^+K^- J/\psi$ [24] final states at BESIII. In addition, a new Y state, the $Y(4500)$, is observed in $e^+e^- \to K^+K^- J/\psi$, recently [24]. Due to no corresponding charmonia predicted in the quark model [25], these Y states are widely recognized as candidates for exotic multiquark hadrons. Possible interpretations include tetra-quarks, hybrid mesons, hadron molecules, hadrocharmonium and threshold effects [26, 27].

One striking feature of these Y states is their large coupling to charmonium final states [28]. In contrast, there is a dip around the known $Y(4230)$ mass in the cross section of $e^+e^- \to$ inclusive hadrons [29] and in the exclusive two-body production of $e^+e^- \to D^{(*)}\bar{D}^{(*)}$ [30, 31]. This is opposite to the behavior of conventional $c\bar{c}$ charmonium states lying above the $D\bar{D}$ mass threshold, which dominantly decays to open-charm final states [1]. Therefore, it is essential to investigate the coupling of the Y states to different open-charm channels to help identify their nature.

In the process $e^+e^- \to D^0 D^{*-}\pi^+$ [20], BESIII first determined a sizable coupling of the $Y(4230)$ with the open-charm $D^0 D^{*-}\pi^+$ decay, which is consistent with the hypothesis of a $D_1(2420)\bar{D}$ molecular state [32–38]. In lattice QCD, the leptonic partial width of the $Y(4230)$, $\Gamma^{ee}_{Y(4230)}$, using a hybrid scenario, is predicted to be less than 40 eV [39]. To date, $\Gamma^{ee}_{Y(4230)}$ is evaluated to be 36.4 ± 4.7 eV, based on the combined analysis of the known $Y(4230)$ decay channels [40]. Study of the $Y(4230)$ in the open-charm process $e^+e^- \to D^*\bar{D}^*\pi$ provides new input to $\Gamma^{ee}_{Y(4230)}$ and to the relative size of different decay modes, which can be used to test the theoretical explanation of the hybrid and $D\bar{D}_1$ molecular state models.

The $Y(4500)$ is reported in the $e^+e^- \to K^+K^- J/\psi$ process [24]. Its spin and mass agree with the predicted baryonium state around 4560 MeV [41]. Furthermore, other theoretical models explain it as a $D_s\bar{D}_{s1}$ molecule, which is a hidden-strangeness partner of the $Y(4230)$ state under the $D\bar{D}_1$ molecule assumption [42], and a charmonium $5S$-$4D$ mixing state [43]. Thus, an independent confirmation in another channel would be important to explore its nature. In addition, since the Born cross section of $e^+e^- \to KZ_{cs}(3985)$ peaks around the $Y(4660)$ mass [44, 45], the $Y(4660)$ is considered to be a hidden-strangeness state. Given that the heavier $Y(4500)$ and $Y(4660)$ states have not been observed in open-charm decay, it is also highly desirable to explore these states in the process $e^+e^- \to D^*\bar{D}^*\pi$ to help determine their quark constituents.

In this Letter, the Born cross sections of the $e^+e^- \to D^{*0}D^{*-}\pi^+ + c.c.$ processes are measured at 86 center-of-mass energies from 4.189 to 4.951 GeV for the first time. The data sets used are accumulated with the BESIII detector at the BEPCII collider and correspond to an integrated luminosity of 17.9 fb^{-1} [46–48]. Details about BEPCII and BESIII can be found in Refs. [49–51]. The data sets include 49 energy points with integrated luminosities less than 10 pb^{-1} ("Scan data") and another 37 energy points with larger integrated luminosities ("XYZ data"). Details of the data sets can be found in Tables I and II of the supplemental material [52]. By fitting the line-shape of dressed cross sections with various hypotheses, we report the observation of three vector charmonium-like Y states in $e^+e^- \to D^{*0}D^{*-}\pi^+ + c.c.$.

Simulated data samples are produced with GEANT4-based [55] Monte Carlo (MC) software, which includes the geometric description [56] of the BESIII detector and the detector response, as detailed in Ref. [51]. The simulation models the beam energy spread and initial state radiation (ISR) in the e^+e^- annihilation with the generator KKMC [57]. The signal MC samples of the $e^+e^- \to \pi^+ D^{*0} D^{*-}$ process are generated according to the partial-wave-analysis results at each energy point. Possible background contributions are estimated by inclusive MC simulation samples, which include the production of open charm processes, the ISR production of vector charmonium(-like) states, and the continuum processes incorporated in KKMC. All particle decays are modeled with EVTGEN [58] using branching fractions (BFs) either taken from the Particle Data Group (PDG) [1], when available, or otherwise estimated with LUNDCHARM [59]. Final state radiation from charged final state particles is incorporated using PHOTOS [60].

To improve the signal selection efficiency, a partial-reconstruction technique is employed to identify the $D^{*0}D^{*-}\pi^+$ final states, in which two tagging methods, the D^0-tag and the D^--tag, are performed. In the $D^0(D^-)$-tag method, the bachelor charged π^+ from primary production, the $D^0(D^-)$ meson and at least one soft $\pi^0(\to\gamma\gamma)$ from $D^{*0}(D^{*-}) \to D^0(D^-)\pi^0$ decay are reconstructed. Here and elsewhere, charge-conjugate modes are always implied. To improve the signal purity, only the decays $D^0 \to K^-\pi^+$, $K^-\pi^+\pi^0$, and $K^-\pi^+\pi^+\pi^-$ ($D^- \to K^+\pi^-\pi^-$), which have relatively large BFs, are reconstructed. By reconstructing the $D^{*0}(D^{*-})$ and the bachelor π^+, the flavor of the missing $D^{*-}(D^{*0})$ meson is fixed. All the charged tracks and π^0 candidates are selected following the criteria in Ref. [61]. To form candidates for $D^0 \to K^-\pi^+$, $D^0 \to K^-\pi^+\pi^0$, $D^0 \to K^-\pi^+\pi^+\pi^-$ and $D^- \to K^+\pi^-\pi^-$ decays, the reconstructed final state invariant masses are required to be within (1.835, 1.887), (1.827, 1.882), (1.855, 1.874) and (1.856, 1.883) GeV/c^2, respectively. Here, the different mass regions are due to the various momentum resolutions. The π^0 candidates from D^* decays can be either from the reconstructed or missing D^* candidates. For the π^0 from missing D^* candidates, its momentum in the reconstructed $D\pi^+$ recoil system, $P^*(\pi^0)$, peaks around $40\,\mathrm{MeV}/c$. To distinguish the source of π^0 with reconstructed D^* candidates, the reconstructed invariant masses are required to satisfy $M(D^0\pi^0) \in (2.004, 2.009)\,\mathrm{GeV}/c^2$ with $P^*(\pi^0) \notin (0.025, 0.050)\,\mathrm{GeV}/c$ in the D^0-tag method, and $M(D^-\pi^0) \in (2.008, 2.013)\,\mathrm{GeV}/c^2$ with $P^*(\pi^0) \notin (0.030, 0.055)\,\mathrm{GeV}/c$ in the D^--tag method, as shown in Fig. 1 for data at $\sqrt{s} = 4.600\,\mathrm{GeV}$. Moreover, the π^+D^0 invariant mass must be greater than $2.02\,\mathrm{GeV}/c^2$ in the D^0-tag method to reject background for the bachelor π^+ from $D^{*+} \to \pi^+D^0$.

To improve the resolution and further suppress the background, a kinematic fit (3C) is performed to constrain the reconstructed π^0, $D^0(D^-)$, and $D^{*0}(D^{*-})$ mesons to their individual known masses [1]. Candidate events are required to have $\chi^2_{3\mathrm{C}} < 50$ and the fitted four-momenta of all related particles are used for further analysis. If there is more than one $\pi^0D^0(D^-)$ candidate in an event, only the one with the minimum $\chi^2_{3\mathrm{C}}$ is retained. Furthermore, if one event survives in both tag methods, only the combination in the D^0-tag method is kept to avoid double counting in the simultaneous fit.

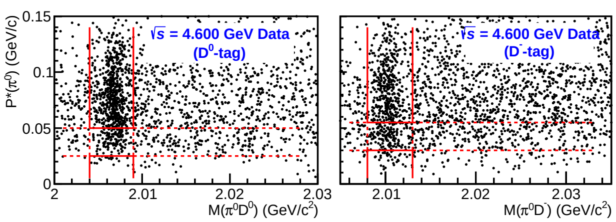

FIG. 1. Two-dimensional distributions of $P^*(\pi^0)$ versus $M(\pi^0D)$ for the D^0-tag (left) and D^--tag (right) methods in data at $\sqrt{s} = 4.600\,\mathrm{GeV}$. The events between the vertical solid lines are kept and those between the horizontal dashed lines are vetoed based on the requirements for $M(\pi^0D)$ and $P^*(\pi^0)$. The distributions for signal MC simulation samples are shown in Fig. 1 of the supplemental material [52].

Figure 2 shows the distributions of the recoil masses of reconstructed π^+, π^0 and D mesons, $RM(\pi^+\pi^0D^0)$ and $RM(\pi^+\pi^0D^-)$. The background study based on inclusive MC simulation samples shows that the shape of the background at each energy point is smooth and can be well described by a second-order Chebyshev function. A peaking background is found in the signal MC simulation due to the mis-combination of particles from the missing and tagged sides. Its shape can be obtained by selecting the unmatched events from inclusive MC simulation samples, in which the missing D^* candidate decays inclusively while the tagged D^* candidate decays into the signal process final state. Its contribution will be fixed in the fit according to the ratio between matched and unmatched events in the MC simulation.

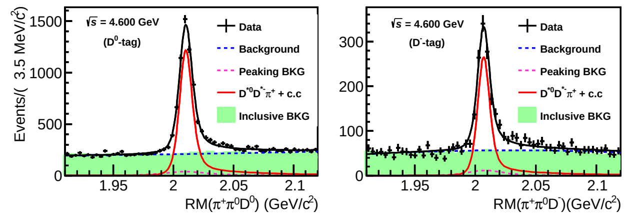

FIG. 2. The distributions of the recoil masses $RM(\pi^+\pi^0D^0)$ (left) and $RM(\pi^+\pi^0D^-)$ (right) for data at $\sqrt{s} = 4.600\,\mathrm{GeV}$ with simultaneous fit results overlaid. The red solid-curve is the signal shape. The pink and blue dashed-curve are the peaking and smooth background, respectively. The light green shadowed histogram is the simulated inclusive background MC samples.

An unbinned extended maximum likelihood fit is performed on the distributions of $RM(\pi^+\pi^0D^0)$ and $RM(\pi^+\pi^0D^-)$ simultaneously to determine the Born cross section at each energy point. Figure 2 shows the fit results at $\sqrt{s} = 4.600\,\mathrm{GeV}$, as an example. The signal shape is derived from MC simulation convolved with a Gaussian function with free parameters to account for the resolution difference between data and MC simulation. The background shape is parameterized as a sum of the shape from unmatched MC samples and a second-order Chebyshev function. The Born cross sections (σ^{Born}) at the individual energy points are calculated by

$$\sigma^{\mathrm{Born}} = \frac{\sigma^{\mathrm{dressed}}}{\frac{1}{|1-\Pi|^2}} = \frac{N^{\mathrm{obs}}_{D^{0(-)}\text{-tag}}}{\mathcal{L}_{\mathrm{int}} \cdot \epsilon_{D^{0(-)}\text{-tag}} \cdot \hat{\mathcal{B}}_{D^{0(-)}\text{-tag}} \cdot (1+\delta^{\mathrm{ISR}}) \cdot \frac{1}{|1-\Pi|^2}}.$$

Here, $N^{\mathrm{obs}}_{D^{0(-)}\text{-tag}}$ is calculated according to σ^{Born} which is taken as a common parameter in the simultaneous fit, $\epsilon_{D^{0(-)}\text{-tag}}$ is the detection efficiency, $\mathcal{L}_{\mathrm{int}}$ is the integral luminosity measured by Refs. [46–48], $\hat{\mathcal{B}}_{D^{0(-)}\text{-tag}}$ stands for an equivalent BF including all the related products of BF obtained from the PDG [1], $(1+\delta^{\mathrm{ISR}})$ and $\frac{1}{|1-\Pi|^2}$ are the correction factors for ISR and vacuum polarization [62]. To estimate the ISR factors and consider the correlation effect on detection efficiencies, an iterative weighting method [63] is performed to correct the corresponding dressed cross section values. All the numerical results from the fits are summarized in Tables I and II of Ref. [52] for the XYZ and Scan data samples, respectively.

The systematic uncertainties in the Born cross section measurements, as detailed in Ref. [52], are divided into three parts. The first part relates to the determination of the detection efficiency, including the tracking, particle identification, π^0 reconstruction, signal region requirements, signal decay model and ISR correction factor. The second part relates to the estimation of signal yields from the fit, consisting of the signal and background shapes as well as the fit range. The last part includes the uncertainties from the luminosities and the intermediate BFs. The items in the first and third parts are completely correlated between different energy points, except for the uncertainties due to signal region requirements and the signal decay model. For the second part at low-yield (< 300 events) energy points, the systematic uncertainties obtained at their nearest energy point in high-yield (> 300 events) XYZ data are used. All the systematic uncertainties are studied for each tag method and combined to obtain the total systematic uncertainties according to their signal yields. The total relative systematic uncertainties at different energy points are between 6.7% to 9.6%.

The dressed cross sections obtained at various energy points are shown in Fig. 3. Three possible enhancements around 4.20, 4.47, and 4.67 GeV are observed. To fit this line-shape, we use the coherent sum of a continuum amplitude for $e^+e^- \to D^{*0}D^{*-}\pi^+ + c.c.$ and three resonance amplitudes described by relativistic Breit-Wigner (BW) functions

$$\sigma^{\rm dressed}(\sqrt{s}) = C_0 \left| C_1\sqrt{\Phi(\sqrt{s})} + \sum_{k=1}^{3} {\rm BW}_k(\sqrt{s}) e^{i\phi_k} \right|^2,$$

where $C_0 = 3.894 \times 10^5\,{\rm nb}\cdot{\rm GeV}^2$ is a unit conversion factor, C_1 is the continuum free parameter, and ϕ_k is the phase angle among different components. The relativistic BW amplitude for a resonance $R_k \to D^{*0}D^{*-}\pi^+$ is written as

$${\rm BW}_k(\sqrt{s}) = \frac{m_k}{\sqrt{s}} \cdot \frac{\sqrt{12\pi\cdot\Gamma_k^{ee}\cdot\mathcal{B}_k\cdot\Gamma_k^{\rm tot}}}{s - m_k^2 + i m_k \Gamma_k^{\rm tot}} \cdot \sqrt{\frac{\Phi(\sqrt{s})}{\Phi(m_k)}},$$

where m_k and $\Gamma_k^{\rm tot}$ are the k-th resonance mass and total width, respectively, $\Gamma_k^{ee}\cdot\mathcal{B}_k$ is the leptonic width of the k-th resonance times the BF of $R_k \to D^{*0}D^{*-}\pi^+ + c.c.$, and $\Phi(\sqrt{s})$ is the three body phase space contribution defined as $\Phi(\sqrt{s}) = \iint \frac{1}{(2\pi)^3 32(\sqrt{s})^3} dm_{23}^2 dm_{12}^2$ [1].

The χ^2 of the fit to the dressed cross section line-shape is constructed according to the method in Ref. [64] by incorporating both the statistical and systematic uncertainty and considering both the correlated and uncorrelated terms. To avoid the bias from correlated systematic uncertainties in the χ^2 minimization [65], the correlated uncertainties are calculated according to the predicted cross section values times the corresponding relative uncertainties when constructing the covariance matrix.

The fit result is shown in Fig. 3. There are eight solutions with the same fit quality with identical continuum contributions as well as masses and widths for the resonances [66]. However, the resulting product $\Gamma_k^{ee}\mathcal{B}_k$ and phases ϕ_k are different, as plotted in Fig. 2 of Ref. [52]. The numerical results are listed in Table I. The dressed cross sections are also fitted under the assumption of only two resonances plus the continuum component. The relative changes in the χ^2 value ($\Delta\chi^2 = 130.5$) and the number of degrees of freedom (Δndof $= 4$) are used to estimate the significance of the three-resonance hypothesis over the two-resonance hypothesis as 10.8σ. The significance of the two-resonance hypothesis over the one-resonance hypothesis is 22.8σ according to the changes of $\Delta\chi^2 = 537.1$ and Δndof $= 4$.

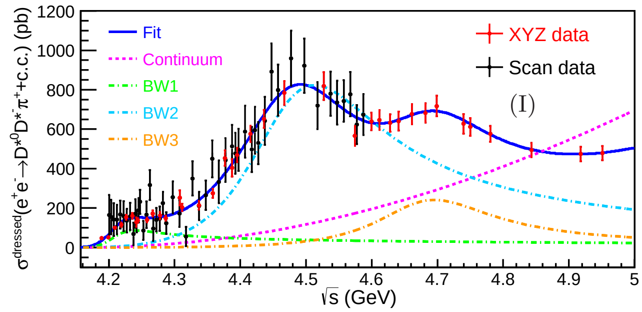

FIG. 3. The fit results (solution I) of the dressed cross section line-shape of $e^+e^- \to D^{*0}D^{*-}\pi^+ + c.c.$. The black points are data, with statistical and systematic uncertainties. The blue curve is the total fit. The green, azure and orange dashed curves describe three BW functions, and the pink dashed-curve is the three body phase space contribution.

The systematic uncertainties of the resonance parameters are mainly from the uncertainties of the center-of-mass energy calibration, beam energy spread and parameterization of the continuum contribution. Other uncertainties from the measured cross sections have been included in the line-shape fit. The uncertainty from the center-of-mass energy measurement is estimated by propagating the largest uncertainty of the measured energies ($0.8\,{\rm MeV}/c^2$) to the Y-state mass parameter. The uncertainty from beam energy spread is considered by smearing the energy with its spread value at each energy point. The differences of resonance parameters determined from fits using nominal and smeared line-shapes are taken as the systematic uncertainties. To estimate the uncertainty related to the fit model, the three body continuum contribution is replaced by a third-order polynomial parameterized function. The resulting differences in the masses and widths of resonances are taken as systematic uncertainties. Assuming the individual systematic uncertainties are uncorrelated, the total systematic uncertainty is obtained by summing the individual values in quadrature, as listed in Table II.

In summary, the Born cross sections of the process $e^+e^- \to D^{*0}D^{*-}\pi^+ + c.c.$ at 86 center-of-mass energies from $\sqrt{s} = 4.189$ to $4.951\,{\rm GeV}$ are measured for the first time with the data samples collected by the BESIII detector. Fitting the dressed cross sections with a three-resonance hypothesis, their masses and widths are determined to be $m_1 = 4209.6 \pm 4.7 \pm 5.9\,{\rm MeV}/c^2$, and $\Gamma_1 = 81.6 \pm 17.8 \pm 9.0\,{\rm MeV}$ (denoted as $Y(4210)$), $m_2 = 4469.1 \pm 26.2 \pm 3.6\,{\rm MeV}/c^2$, and $\Gamma_2 = 246.3 \pm 36.7 \pm 9.4\,{\rm MeV}$ (denoted as $Y(4470)$), $m_3 = 4675.3 \pm 29.5 \pm 3.5\,{\rm MeV}/c^2$, and $\Gamma_3 = 218.3 \pm 72.9 \pm 9.3\,{\rm MeV}$

TABLE I. The fit results of the dressed cross section line-shape of $e^+e^- \to D^{*0}D^{*-}\pi^+ + c.c.$ with eight different solutions. For the uncertainties of the masses and widths, those from the solutions with maximum uncertainties are adopted.

	I	II	III	IV	V	VI	VII	VIII
C_1 (10^{-3})	4.2 ± 1.5							
m_1 (MeV/c^2)	4209.6 ± 4.7							
$\Gamma_1^{\rm tot}$ (MeV)	81.6 ± 17.8							
$\Gamma_1^{ee}\mathcal{B}_1$ (eV)	5.4 ± 1.1	6.0 ± 1.3	4.8 ± 0.9	5.3 ± 1.1	17.9 ± 7.2	19.8 ± 6.6	20.2 ± 7.4	22.4 ± 9.0
ϕ_1 (rad)	3.1 ± 0.5	3.8 ± 0.4	1.9 ± 0.7	2.6 ± 0.6	4.2 ± 0.3	4.8 ± 0.2	5.4 ± 0.3	6.0 ± 0.3
m_2 (MeV/c^2)	4469.1 ± 26.2							
$\Gamma_2^{\rm tot}$ (MeV)	246.3 ± 36.7							
$\Gamma_2^{ee}\mathcal{B}_2$ (eV)	243.3 ± 83.5	832.5 ± 716.5	107.4 ± 50.6	367.4 ± 370.8	225.5 ± 94.9	770.8 ± 383.8	510.1 ± 202.3	1744.3 ± 926.9
ϕ_2 (rad)	4.4 ± 0.3	-0.9 ± 0.3	2.6 ± 0.6	3.7 ± 0.8	1.9 ± 0.8	3.0 ± 0.4	3.7 ± 0.3	-1.5 ± 0.3
m_3 (MeV/c^2)	4675.3 ± 29.5							
$\Gamma_3^{\rm tot}$ (MeV)	218.3 ± 72.9							
$\Gamma_3^{ee}\mathcal{B}_3$ (eV)	75.8 ± 148.8	1601.9 ± 1152.6	19.4 ± 27.1	411.6 ± 230.5	24.4 ± 34.5	515.6 ± 244.6	95.1 ± 173.1	2005.3 ± 1166.1
ϕ_3 (rad)	4.9 ± 1.4	-2.9 ± 0.4	2.1 ± 0.4	0.6 ± 1.1	1.7 ± 0.5	6.5 ± 0.5	4.5 ± 1.3	-3.3 ± 0.3

TABLE II. The systematic uncertainties in the measurements of the Y-state parameters.

Source	Energy	Beam spread	Fit model	Total
m_1(MeV/c^2)	0.8	5.5	2.0	5.9
$\Gamma_1^{\rm tot}$(MeV)	-	1.7	8.8	9.0
m_2(MeV/c^2)	0.8	3.5	0.7	3.6
$\Gamma_2^{\rm tot}$(MeV)	-	6.9	6.4	9.4
m_3(MeV/c^2)	0.8	1.5	3.1	3.5
$\Gamma_3^{\rm tot}$(MeV)	-	7.4	5.7	9.3

(denoted as $Y(4660)$), where the first uncertainties are statistical and the second are systematic. The significance of the three-resonance hypothesis compared with the two-resonance one is greater than 10σ. The mass of $Y(4210)$ is consistent with the mass of $Y(4230)$ from the combined fit in Ref. [40]. If we assume they are the same resonance, $\Gamma^{ee}_{Y(4230)}$ becomes greater than 40 eV, which disfavors the hybrid interpretation under the lattice QCD calculation [39]. In addition, we find the couplings of $Y(4230)$ to $D^{*0}D^{*-}\pi^+$ and $D^0D^{*-}\pi^+$ are at the same order of magnitude. This is the first observation of the state $Y(4470)$ in an open-charm process, and its resonance parameters are compatible with those of the $Y(4500)$ state observed in $e^+e^- \to K^+K^-J/\psi$ [24]. Assuming the $Y(4470)$ and $Y(4500)$ are the same state, the rate of its decay to $D^*\bar{D}^*\pi$ is two orders of magnitude greater than that to $K\bar{K}J/\psi$, which is inconsistent with the conjecture of hidden-strangeness enhancement of the Y(4500) [42]. We confirm for the first time the existence of the resonance $Y(4660)$ in open-charm final states with resonance parameters consistent with the latest results derived in $e^+e^- \to \pi^+\pi^-\psi(2S)$ at BESIII [14]. However, the relative size of their couplings can not be constrained by current data, as different fit solutions result in large variations of the product $\Gamma^{ee}_{Y(4660)}\mathcal{B}_{Y(4660)}$. Further amplitude analyses of different open- and hidden-charm final states are desired to advance our knowledge of the nature of these Y states.

The BESIII collaboration thanks the staff of BEPCII and the IHEP computing center for their strong support. This work is supported in part by National Key R&D Program of China under Contracts Nos. 2020YFA0406400, 2020YFA0406300; National Natural Science Foundation of China (NSFC) under Contracts Nos. 11635010, 11735014, 11835012, 11935015, 11935016, 11935018, 11961141012, 12022510, 12025502, 12035009, 12035013, 12061131003, 12192260, 12192261, 12192262, 12192263, 12192264, 12192265, 12221005; the Chinese Academy of Sciences (CAS) Large-Scale Scientific Facility Program; the CAS Center for Excellence in Particle Physics (CCEPP); Joint Large-Scale Scientific Facility Funds of the NSFC and CAS under Contract No. U1832207; CAS Key Research Program of Frontier Sciences under Contracts Nos. QYZDJ-SSW-SLH003, QYZDJ-SSW-SLH040; 100 Talents Program of CAS; Fundamental Research Funds for the Central Universities, Lanzhou University, University of Chinese Academy of Sciences; The Institute of Nuclear and Particle Physics (INPAC) and Shanghai Key Laboratory for Particle Physics and Cosmology; ERC under Contract No. 758462; European Union's Horizon 2020 research and innovation programme under Marie Sklodowska-Curie grant agreement under Contract No. 894790; German Research Foundation DFG under Contracts Nos. 443159800, 455635585, Collaborative Research Center CRC 1044, FOR5327, GRK 2149; Istituto Nazionale di Fisica Nucleare, Italy; Ministry of Development of Turkey under Contract No. DPT2006K-120470; National Research Foundation of Korea under Contract No. NRF-2022R1A2C1092335; National Science and Technology fund; National Science Research and Innovation Fund (NSRF) via the Program Management Unit for Human Resources & Institutional Development, Research and Innovation under Contract No. B16F640076; Polish National Science Centre under Contract No. 2019/35/O/ST2/02907; Suranaree University of Technology (SUT), Thailand Science Research and Innovation (TSRI), and National Science Research and Innovation Fund (NSRF) under Contract No. 160355; The Royal Society, UK under Contract No. DH160214; The Swedish Research Council; U. S. Department of Energy under Contract No. DE-FG02-05ER41374.

---

[1] R. L. Workman (Particle Data Group), PTEP **2022**, 083C01 (2022).

[2] B. Aubert *et al.* (BaBar Collaboration), Phys. Rev. Lett. **95**, 142001 (2005).

[3] Q. He *et al.* (CLEO Collaboration), Phys. Rev. D **74**, 091104 (2006).

[4] C. Z. Yuan *et al.* (Belle Collaboration), Phys. Rev. Lett. **99**, 182004 (2007).

[5] M. Ablikim *et al.* (BESIII Collaboration), Phys. Rev. Lett. **118**, 092001 (2017).

[6] M. Ablikim *et al.* (BESIII Collaboration), Phys. Rev. D **102**, 012009 (2020).

[7] M. Ablikim *et al.* (BESIII Collaboration), Phys. Rev. D **106**, 072001(2022).

[8] B. Aubert *et al.* (BaBar Collaboration), Phys. Rev. Lett. **98**, 212001 (2007).

[9] J. P. Lees *et al.* (BaBar Collaboration), Phys. Rev. D **89**, 111103 (2014).

[10] X. L. Wang *et al.* (Belle Collaboration), Phys. Rev. Lett. **99**, 142002 (2007).

[11] X. L. Wang *et al.* (Belle Collaboration), Phys. Rev. D **91**, 112007 (2015).

[12] M. Ablikim *et al.* (BESIII Collaboration), Phys. Rev. D **96**, 032004 (2017) [erratum: Phys. Rev. D **99**, 019903 (2019)].

[13] M. Ablikim *et al.* (BESIII Collaboration), Phys. Rev. D **97**, 052001 (2018).

[14] M. Ablikim *et al.* (BESIII Collaboration), Phys. Rev. D **104**, 052012 (2021).

[15] M. Ablikim *et al.* (BESIII Collaboration), Phys. Rev. Lett. **118**, 092002 (2017).

[16] M. Ablikim *et al.* (BESIII Collaboration), Phys. Rev. Lett. **114**, 092003 (2015).

[17] M. Ablikim *et al.* (BESIII Collaboration), Phys. Rev. D **99**, 091103 (2019).

[18] M. Ablikim *et al.* (BESIII Collaboration), Phys. Rev. D **102**, 031101 (2020).

[19] M. Ablikim *et al.* (BESIII Collaboration), Phys. Rev. D **101**, 012008 (2020).

[20] M. Ablikim *et al.* (BESIII Collaboration), Phys. Rev. Lett. **122**, 102002 (2019).

[21] M. Ablikim *et al.* (BESIII Collaboration), Phys. Rev. Lett. **129**, 102003 (2022).

[22] M. Ablikim *et al.* (BESIII Collaboration), Phys. Lett. B **804**, 135395 (2020).

[23] M. Ablikim *et al.* (BESIII Collaboration), Phys. Rev. D **106**, 052012 (2022).

[24] M. Ablikim *et al.* (BESIII Collaboration), Chin. Phys. C **46**, 111002 (2022).

[25] T. Barnes, S. Godfrey and E. S. Swanson, Phys. Rev. D **72**, 054026 (2005).

[26] H. X. Chen, W. Chen, X. Liu and S. L. Zhu, Phys. Rept. **639**, 1 (2016).

[27] F. K. Guo, C. Hanhart, U. G. Meißner, Q. Wang, Q. Zhao and B. S. Zou, Rev. Mod. Phys. **90**, 015004 (2018) [erratum: Rev. Mod. Phys. **94**, 029901 (2022)].

[28] C. Z. Yuan, Natl. Sci. Rev. **8**, nwab182 (2021).

[29] J. Z. Bai *et al.* (BES Collaboration), Phys. Rev. Lett. **88**, 101802 (2002).

[30] R. A. Briceno *et al.*, Chin. Phys. C **40**, 042001 (2016).

[31] M. Ablikim *et al.* (BESIII Collaboration), JHEP **05**, 155 (2022).

[32] M. Cleven, Q. Wang, F. K. Guo, C. Hanhart, U. G. Meißner and Q. Zhao, Phys. Rev. D **90**, 074039 (2014).

[33] G. J. Ding, Phys. Rev. D **79**, 014001 (2009).

[34] G. Li and X. H. Liu, Phys. Rev. D **88**, 094008 (2013).

[35] M. T. Li, W. L. Wang, Y. B. Dong and Z. Y. Zhang, [arXiv:1303.4140 [nucl-th]].

[36] Q. Wang, C. Hanhart and Q. Zhao, Phys. Rev. Lett. **111**, 132003 (2013).

[37] X. G. Wu, C. Hanhart, Q. Wang and Q. Zhao, Phys. Rev. D **89**, 054038 (2014).

[38] T. Ji, X. K. Dong, F. K. Guo and B. S. Zou, Phys. Rev. Lett. **129**, 102002 (2022).

[39] Y. Chen, W. F. Chiu, M. Gong, L. C. Gui and Z. Liu, Chin. Phys. C **40**, 081002 (2016).

[40] J. Zhang, L. Yuan and R. Wang, Adv. High Energy Phys. **2018**, 5428734 (2018).

[41] C. F. Qiao, J. Phys. G **35**, 075008 (2008).

[42] F. Z. Peng, M. J. Yan, M. Sánchez Sánchez and M. Pavon Valderrama, Phys. Rev. D **107**, 016001 (2023).

[43] J. Z. Wang and X. Liu, [arXiv:2212.13512 [hep-ph]].

[44] M. Ablikim *et al.* (BESIII Collaboration), Phys. Rev. Lett. **126**, 102001 (2021).

[45] M. Ablikim *et al.* (BESIII Collaboration), Phys. Rev. Lett. **129**, 112003 (2022).

[46] M. Ablikim *et al.* (BESIII Collaboration), Chin. Phys. C **41**, 063001 (2017).

[47] M. Ablikim *et al.* (BESIII Collaboration), Chin. Phys. C **45**, 103001 (2021).

[48] M. Ablikim *et al.* (BESIII Collaboration), Chin. Phys. C **46**, 113003 (2022).

[49] C. H. Yu *et al.*, Proceedings of IPAC2016, Busan, Korea, 2016.

[50] M. Ablikim *et al.* (BESIII Collaboration), Nucl. Instrum. Meth. A **614**, 345 (2010).

[51] M. Ablikim *et al.* (BESIII Collaboration), Chin. Phys. C **44**, 040001 (2020).

[52] See Supplemental Material at [link to be added] for additional analysis information, which includes Refs. [1, 46–48, 53, 54].

[53] M. Ablikim *et al.* (BESIII Collaboration), Phys. Rev. D **83**, 112005 (2011).

[54] M. Ablikim *et al.* (BESIII Collaboration), Phys. Rev. D **81**, 052005 (2010).

[55] S. Agostinelli *et al.* (GEANT4 Collaboration), Nucl. Instrum. Meth. A **506**, 250 (2003).

[56] K. X. Huang, Z. J. Li, Z. Qian, J. Zhu, H. Y. Li, Y. M. Zhang, S. S. Sun and Z. Y. You, Nucl. Sci. Tech. **33**, no.11, 142 (2022).
[57] S. Jadach, B. F. L. Ward and Z. Was, Phys. Rev. D **63**, 113009 (2001); Comput. Phys. Commun. **130**, 260 (2000).
[58] D. J. Lange, Nucl. Instrum. Meth. A **462**, 152 (2001); R. G. Ping, Chin. Phys. C **32**, 599 (2008).
[59] J. C. Chen, G. S. Huang, X. R. Qi, D. H. Zhang and Y. S. Zhu, Phys. Rev. D **62**, 034003 (2000); R. L. Yang, R. G. Ping and H. Chen, Chin. Phys. Lett. **31**, 061301 (2014).
[60] E. Richter-Was, Phys. Lett. B **303**, 163 (1993).
[61] M. Ablikim *et al.* (BESIII Collaboration), Phys. Rev. Lett. **112**, 132001 (2014).
[62] F. Jegerlehner, Nuovo Cim. C **034S1**, 31-40 (2011).
[63] W. Sun, T. Liu, M. Jing, L. Wang, B. Zhong and W. Song, Front. Phys. (Beijing) **16**, 64501 (2021).
[64] M. Ablikim *et al.* (BESIII Collaboration), Phys. Rev. D **103**, 072007 (2021).
[65] W. M. Sun, Nucl. Instrum. Meth. A **556**, 325 (2006).
[66] Y. Bai and D. Y. Chen, Phys. Rev. D **99**, 072007 (2019).

Supplemental Material for "Observation of Three Charmonium-like States with $J^{PC} = 1^{--}$ in $e^+e^- \to D^{*0}D^{*-}\pi^+ + c.c.$ Process"

Appendix A: Details on event selection

Two-dimensional distributions of $P^*(\pi^0)$ versus $M(\pi^0 D)$ for MC samples with D^0-tag and D^--tag methods at $\sqrt{s} = 4.600\,\text{GeV}$ are shown in Fig. 1, respectively.

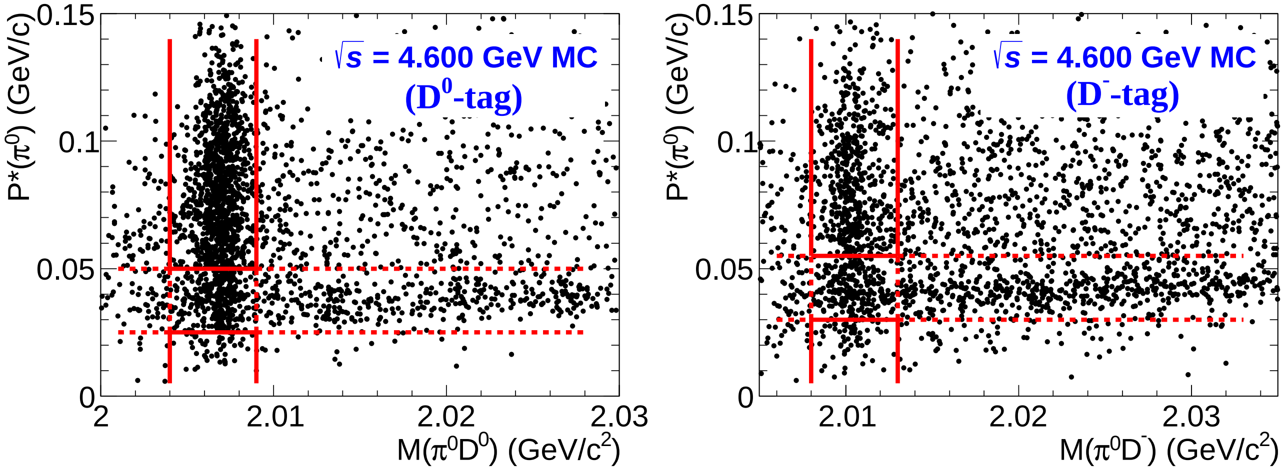

FIG. 1. Two-dimensions distributions of $P^*(\pi^0)$ versus $M(\pi^0 D)$ for MC simulation with D^0-tag and D^--tag methods at $\sqrt{s} = 4.600\,\text{GeV}$. The events are kept inside the vertical solid lines and vetoed inside the horizontal dashed lines based on the requirements for $M(\pi^0 D)$ and $P^*(\pi^0)$.

Appendix B: Signal yields and Born cross section

A simultaneous fit of D^0-tag and D^--tag is performed at each energy point according to the calculation of Born cross section.

$$\sigma^{\text{Born}} = \frac{\sigma^{\text{dressed}}}{\frac{1}{|1-\Pi|^2}} = \frac{N^{\text{obs}}_{D^{0(-)}\text{-tag}}}{\mathcal{L}_{\text{int}} \cdot \epsilon_{D^{0(-)}\text{-tag}} \cdot \hat{\mathcal{B}}_{D^{0(-)}\text{-tag}} \cdot (1+\delta^{\text{ISR}}) \cdot \frac{1}{|1-\Pi|^2}}.$$

The the integral luminosities $\mathcal{L}_{\text{int}}$ are measured by Refs. [46–48]. The σ^{Born} is taken as a common parameter in the fitting while detection efficiencies, ISR and vacuum polarization factors are estimated based on MC simulation. With the fit results shown in Tables I and II, $N^{\text{obs}}_{D^0\text{-tag}}$ and $N^{\text{obs}}_{D^-\text{-tag}}$ can be calculated directly.

TABLE I. The Born cross section of $e^+e^- \to D^{*0}D^{*-}\pi^+ + c.c.$ for XYZ data sets. The first uncertainties are statistical and the second ones systematic.

$\sqrt{s}$ (GeV)	$\mathcal{L}_{\rm int}$ (pb^{-1})	$1+\delta^{\rm ISR}$	$\frac{1}{\lvert 1-\Pi\rvert^2}$	$N^{\rm obs}_{D^0\text{-tag}}$	$\epsilon_{D^0\text{-tag}}$ (%)	$N^{\rm obs}_{D^-\text{-tag}}$	$\epsilon_{D^-\text{-tag}}$ (%)	$\sigma^{\rm Born}$ (pb)
4.189	570.0	0.667	1.056	32.0 ± 5.5	1.1	8.3 ± 1.4	1.6	$44.9 \pm 7.8 \pm 3.5$
4.199	526.6	0.675	1.056	62.6 ± 8.6	2.0	13.4 ± 1.8	2.6	$48.5 \pm 6.7 \pm 3.8$
4.209	572.1	0.696	1.057	193.3 ± 14.2	2.9	37.5 ± 2.7	3.3	$94.4 \pm 6.9 \pm 7.5$
4.219	569.2	0.726	1.056	291.0 ± 17.1	3.6	55.0 ± 3.2	4.0	$110.2 \pm 6.5 \pm 8.7$
4.226	1111.9	0.749	1.056	1173.5 ± 34.9	4.3	173.9 ± 5.2	4.8	$145.6 \pm 4.3 \pm 11.5$
4.236	530.3	0.770	1.056	468.0 ± 24.1	4.2	88.5 ± 4.6	4.8	$151.7 \pm 7.8 \pm 11.5$
4.242	55.9	0.780	1.055	51.6 ± 8.9	5.4	9.7 ± 1.7	6.1	$122.3 \pm 21.2 \pm 8.5$
4.244	538.1	0.784	1.056	522.4 ± 26.6	5.3	98.5 ± 5.0	6.0	$130.4 \pm 6.6 \pm 9.0$
4.258	828.4	0.795	1.054	1077.9 ± 37.9	5.5	162.8 ± 5.7	6.2	$132.6 \pm 4.7 \pm 10.8$
4.267	531.1	0.797	1.053	571.3 ± 28.2	4.6	109.5 ± 5.4	5.3	$163.6 \pm 8.1 \pm 11.6$
4.278	175.7	0.802	1.053	177.7 ± 16.1	4.6	34.1 ± 3.1	5.2	$153.7 \pm 13.9 \pm 10.9$
4.287	494.2	0.802	1.053	578.5 ± 27.7	5.8	109.9 ± 5.3	6.5	$141.8 \pm 6.8 \pm 10.4$
4.308	45.1	0.802	1.052	85.0 ± 11.1	5.5	16.3 ± 2.1	6.3	$239.0 \pm 31.3 \pm 19.1$
4.311	494.3	0.802	1.052	745.5 ± 33.2	5.5	143.8 ± 6.4	6.3	$193.7 \pm 8.6 \pm 15.5$
4.337	506.1	0.799	1.051	1078.9 ± 42.2	7.4	201.5 ± 7.9	8.2	$203.7 \pm 8.0 \pm 19.6$
4.358	543.9	0.798	1.051	1604.8 ± 50.2	8.0	304.4 ± 9.5	9.0	$262.3 \pm 8.2 \pm 20.1$
4.377	524.7	0.796	1.051	1909.7 ± 55.2	6.0	367.6 ± 10.6	6.8	$431.5 \pm 12.5 \pm 35.9$
4.387	55.6	0.794	1.051	234.1 ± 19.2	7.8	45.2 ± 3.7	8.9	$384.3 \pm 31.5 \pm 28.0$
4.395	508.2	0.792	1.051	2421.6 ± 60.0	7.6	466.1 ± 11.5	8.7	$446.5 \pm 11.1 \pm 32.5$
4.416	1090.7	0.794	1.052	6225.0 ± 95.7	7.4	1185.2 ± 18.2	8.3	$547.7 \pm 8.4 \pm 38.5$
4.436	570.6	0.796	1.054	3798.9 ± 74.6	7.6	755.4 ± 14.8	9.0	$619.3 \pm 12.2 \pm 42.2$
4.467	111.1	0.810	1.055	929.9 ± 35.9	7.8	176.2 ± 6.8	8.8	$742.9 \pm 28.7 \pm 50.8$
4.527	112.1	0.863	1.054	1128.2 ± 39.2	8.4	217.5 ± 7.5	9.7	$776.7 \pm 27.0 \pm 60.5$
4.575	48.9	0.900	1.054	430.3 ± 25.1	10.2	86.1 ± 5.0	12.1	$537.1 \pm 31.4 \pm 36.4$
4.600	586.9	0.905	1.055	5964.6 ± 95.1	10.4	1206.9 ± 19.2	12.5	$606.4 \pm 9.7 \pm 41.2$
4.613	103.7	0.906	1.055	1019.2 ± 38.9	9.9	210.1 ± 8.0	12.1	$613.4 \pm 23.4 \pm 41.2$
4.628	521.5	0.902	1.054	5115.1 ± 88.6	10.2	1026.4 ± 17.8	12.1	$599.2 \pm 10.4 \pm 40.5$
4.641	551.7	0.901	1.054	5404.6 ± 90.2	10.0	1123.5 ± 18.7	12.4	$608.4 \pm 10.1 \pm 44.4$
4.661	529.4	0.895	1.054	5434.9 ± 91.8	10.1	1111.6 ± 18.8	12.2	$641.7 \pm 10.8 \pm 47.1$
4.682	1667.4	0.896	1.054	18143.7 ± 168.0	10.6	3743.9 ± 34.7	12.9	$647.2 \pm 6.0 \pm 45.3$
4.699	535.5	0.900	1.055	6088.0 ± 97.2	10.4	1265.0 ± 20.2	12.9	$680.3 \pm 10.9 \pm 48.9$
4.740	163.9	0.925	1.055	1761.7 ± 54.3	11.0	374.8 ± 11.5	13.9	$595.0 \pm 18.3 \pm 43.3$
4.750	366.6	0.934	1.055	3902.4 ± 80.9	11.0	824.4 ± 17.1	13.8	$580.0 \pm 12.0 \pm 40.9$
4.781	511.5	0.957	1.055	5185.2 ± 95.2	10.9	1113.7 ± 20.4	13.9	$546.8 \pm 10.0 \pm 36.6$
4.843	525.2	0.979	1.056	4539.6 ± 91.7	10.6	972.9 ± 19.7	13.4	$468.4 \pm 9.5 \pm 33.1$
4.918	207.8	0.973	1.056	1674.8 ± 55.2	10.4	370.3 ± 12.2	13.6	$448.7 \pm 14.8 \pm 31.8$
4.951	159.3	0.965	1.056	1273.9 ± 39.5	10.3	283.3 ± 8.8	13.5	$452.9 \pm 14.1 \pm 31.1$

TABLE II. The Born cross section of $e^+e^- \to D^{*0}D^{*-}\pi^+ + c.c.$ for Scan data sets. The first uncertainties are statistical and the second ones systematic.

$\sqrt{s}$ (GeV)	$\mathcal{L}_{\rm int}$ (pb^{-1})	$1+\delta^{\rm ISR}$	$\frac{1}{\lvert 1-\Pi\rvert^2}$	$N^{\rm obs}_{D^0\text{-tag}}$	$\epsilon_{D^0\text{-tag}}$ (%)	$N^{\rm obs}_{D^-\text{-tag}}$	$\epsilon_{D^-\text{-tag}}$ (%)	$\sigma^{\rm Born}$ (pb)
4.200	6.8	0.677	1.057	2.9 ± 1.5	2.3	0.6 ± 0.3	2.8	$156.2 \pm 81.6 \pm 12.3$
4.203	7.6	0.681	1.057	3.4 ± 1.6	2.5	0.7 ± 0.3	3.0	$146.3 \pm 71.0 \pm 11.5$
4.207	7.7	0.691	1.057	3.7 ± 1.9	2.9	0.7 ± 0.4	3.3	$134.3 \pm 68.0 \pm 10.6$
4.212	7.8	0.705	1.057	4.2 ± 1.9	3.2	0.8 ± 0.4	3.8	$134.6 \pm 61.2 \pm 10.6$
4.217	7.9	0.720	1.056	6.0 ± 2.2	3.8	1.1 ± 0.4	4.1	$158.1 \pm 58.7 \pm 13.0$
4.222	8.2	0.738	1.056	6.5 ± 2.8	4.0	1.2 ± 0.5	4.4	$150.2 \pm 64.5 \pm 11.8$
4.227	8.2	0.751	1.056	5.9 ± 2.3	4.2	1.1 ± 0.4	4.7	$128.8 \pm 50.7 \pm 10.1$
4.232	8.3	0.762	1.056	7.0 ± 2.7	4.2	1.3 ± 0.5	4.7	$148.8 \pm 58.0 \pm 11.7$
4.237	7.8	0.773	1.055	3.5 ± 2.6	5.0	0.7 ± 0.5	5.7	$65.0 \pm 47.7 \pm 4.5$
4.240	8.6	0.778	1.055	10.0 ± 3.8	5.2	1.8 ± 0.7	5.6	$163.5 \pm 61.9 \pm 11.3$
4.242	8.5	0.781	1.056	8.1 ± 3.0	5.5	1.5 ± 0.5	5.9	$125.4 \pm 46.9 \pm 8.7$
4.245	8.6	0.784	1.056	11.7 ± 3.5	5.5	2.2 ± 0.6	6.0	$179.1 \pm 52.8 \pm 12.4$
4.247	8.6	0.787	1.055	14.9 ± 3.5	5.6	2.7 ± 0.6	6.2	$219.5 \pm 51.4 \pm 15.2$
4.252	8.7	0.792	1.054	5.3 ± 2.6	5.3	1.0 ± 0.5	5.9	$81.9 \pm 40.7 \pm 6.6$
4.257	8.9	0.795	1.054	10.7 ± 3.9	5.4	2.1 ± 0.8	6.2	$157.6 \pm 57.9 \pm 12.8$
4.262	8.6	0.796	1.053	16.9 ± 3.6	4.6	3.2 ± 0.7	5.1	$300.1 \pm 64.4 \pm 21.2$
4.267	8.6	0.798	1.053	5.2 ± 3.1	4.7	1.0 ± 0.6	5.2	$90.8 \pm 54.2 \pm 6.4$
4.272	8.6	0.800	1.053	7.7 ± 2.9	4.7	1.5 ± 0.6	5.4	$133.5 \pm 51.1 \pm 9.4$
4.277	8.7	0.800	1.053	10.2 ± 3.9	5.9	1.9 ± 0.7	6.6	$139.0 \pm 53.3 \pm 9.8$
4.282	8.6	0.803	1.053	16.0 ± 3.6	6.1	3.0 ± 0.7	6.7	$214.0 \pm 48.9 \pm 20.8$
4.287	9.0	0.802	1.053	9.1 ± 3.7	6.1	1.7 ± 0.7	6.7	$117.6 \pm 47.5 \pm 11.4$
4.297	8.5	0.801	1.052	15.9 ± 4.6	5.5	2.9 ± 0.8	5.9	$242.0 \pm 70.1 \pm 19.3$
4.307	8.6	0.803	1.052	10.9 ± 3.9	5.4	2.1 ± 0.7	6.1	$163.2 \pm 57.9 \pm 13.0$
4.317	9.3	0.801	1.052	3.7 ± 3.6	5.9	0.7 ± 0.7	6.5	$53.4 \pm 46.1 \pm 3.7$
4.327	8.7	0.800	1.051	30.2 ± 6.6	7.4	5.7 ± 1.2	8.2	$333.1 \pm 72.2 \pm 31.9$
4.337	8.7	0.798	1.051	18.2 ± 5.6	7.4	3.4 ± 1.1	8.3	$199.9 \pm 61.8 \pm 19.2$
4.347	8.5	0.798	1.051	23.8 ± 6.1	7.8	4.3 ± 1.1	8.4	$251.9 \pm 64.7 \pm 19.2$
4.357	8.1	0.797	1.051	36.9 ± 6.8	7.6	6.9 ± 1.3	8.4	$428.1 \pm 79.2 \pm 32.7$
4.367	8.5	0.796	1.051	23.0 ± 6.9	6.1	4.2 ± 1.3	6.6	$316.5 \pm 94.4 \pm 26.3$
4.377	8.2	0.796	1.051	29.9 ± 6.7	6.2	5.7 ± 1.3	7.0	$421.9 \pm 94.8 \pm 35.0$
4.387	7.5	0.794	1.051	40.2 ± 7.8	7.9	7.3 ± 1.4	8.5	$487.6 \pm 94.2 \pm 35.4$
4.392	7.4	0.794	1.051	37.5 ± 7.4	7.9	7.2 ± 1.4	8.9	$454.6 \pm 89.3 \pm 33.0$
4.397	7.2	0.793	1.051	38.3 ± 7.5	8.0	7.2 ± 1.4	9.0	$471.3 \pm 92.1 \pm 34.2$
4.407	6.4	0.793	1.052	36.3 ± 7.4	7.3	6.9 ± 1.4	8.2	$558.4 \pm 113.5 \pm 39.0$
4.417	7.5	0.793	1.052	37.4 ± 7.8	7.5	7.1 ± 1.5	8.4	$473.1 \pm 99.3 \pm 33.1$
4.422	7.4	0.793	1.052	43.9 ± 7.9	7.4	8.3 ± 1.5	8.3	$564.9 \pm 101.8 \pm 39.5$
4.427	6.8	0.794	1.053	42.0 ± 7.7	8.7	8.1 ± 1.5	9.9	$503.3 \pm 91.9 \pm 34.2$
4.437	7.6	0.796	1.054	52.5 ± 9.0	8.0	10.3 ± 1.8	9.3	$609.9 \pm 104.1 \pm 41.4$
4.447	7.7	0.800	1.054	67.7 ± 9.5	7.3	12.8 ± 1.8	8.2	$845.9 \pm 118.8 \pm 57.5$
4.457	8.7	0.803	1.055	69.9 ± 9.9	7.4	13.5 ± 1.9	8.5	$756.7 \pm 107.2 \pm 51.5$
4.477	8.2	0.816	1.055	85.4 ± 10.6	7.9	15.6 ± 1.9	8.6	$909.9 \pm 113.2 \pm 61.9$
4.497	8.0	0.833	1.055	81.6 ± 10.5	7.9	15.6 ± 2.0	8.9	$874.1 \pm 112.4 \pm 59.5$
4.517	8.7	0.855	1.055	73.6 ± 10.5	8.2	13.9 ± 2.0	9.2	$682.5 \pm 97.1 \pm 53.0$
4.537	9.3	0.875	1.054	101.3 ± 11.9	9.4	20.1 ± 2.4	11.1	$739.8 \pm 87.2 \pm 57.5$
4.547	8.8	0.884	1.054	92.0 ± 11.5	9.6	18.2 ± 2.3	11.2	$697.0 \pm 87.3 \pm 54.2$
4.557	8.3	0.892	1.054	90.9 ± 11.0	9.8	17.9 ± 2.2	11.5	$704.7 \pm 85.2 \pm 47.7$
4.567	8.4	0.897	1.054	96.5 ± 12.0	9.8	19.0 ± 2.4	11.4	$737.6 \pm 91.5 \pm 49.9$
4.577	8.5	0.901	1.055	78.7 ± 10.9	9.7	15.8 ± 2.2	11.6	$591.7 \pm 82.3 \pm 40.0$
4.587	8.2	0.905	1.055	83.3 ± 11.3	9.9	16.6 ± 2.2	11.7	$639.5 \pm 86.4 \pm 43.3$

Appendix C: Multiple solutions of line-shape fit

The dressed cross section is parameterized as the coherent sum of a continuum amplitude for $e^+e^- \to D^{*0}D^{*-}\pi^+ + c.c.$ and three resonance amplitudes described by relativistic Breit-Wigner functions:

$$\sigma^{\rm dressed}(\sqrt{s}) = C_0|C_1\sqrt{\Phi(\sqrt{s})} + \sum_{k=1}^{3}{\rm BW}_k(\sqrt{s})e^{i\phi_k}|^2,$$

with relativistic Breit-Wigner amplitude for a resonance $R_k \to D^{*0}D^{*-}\pi^+$,

$${\rm BW}_k(\sqrt{s}) = \frac{m_k}{\sqrt{s}} \cdot \frac{\sqrt{12\pi \cdot \Gamma_k^{ee}\mathcal{B}_k \cdot \Gamma_k^{\rm tot}}}{s - m_k^2 + im_k\Gamma_k^{\rm tot}} \cdot \sqrt{\frac{\Phi(\sqrt{s})}{\Phi(m_k)}},$$

and 3-body phase space contribution $\Phi(\sqrt{s}) = \iint \frac{1}{(2\pi)^3 32(\sqrt{s})^3} dm_{23}^2 dm_{12}^2$. All the parameters in the fit are free except for $C_0 = 3.894 \times 10^5\,{\rm nb} \cdot {\rm GeV}^2$ as a unit conversion factor. There are eight solutions with the same fit quality, as shown in Fig. 2.

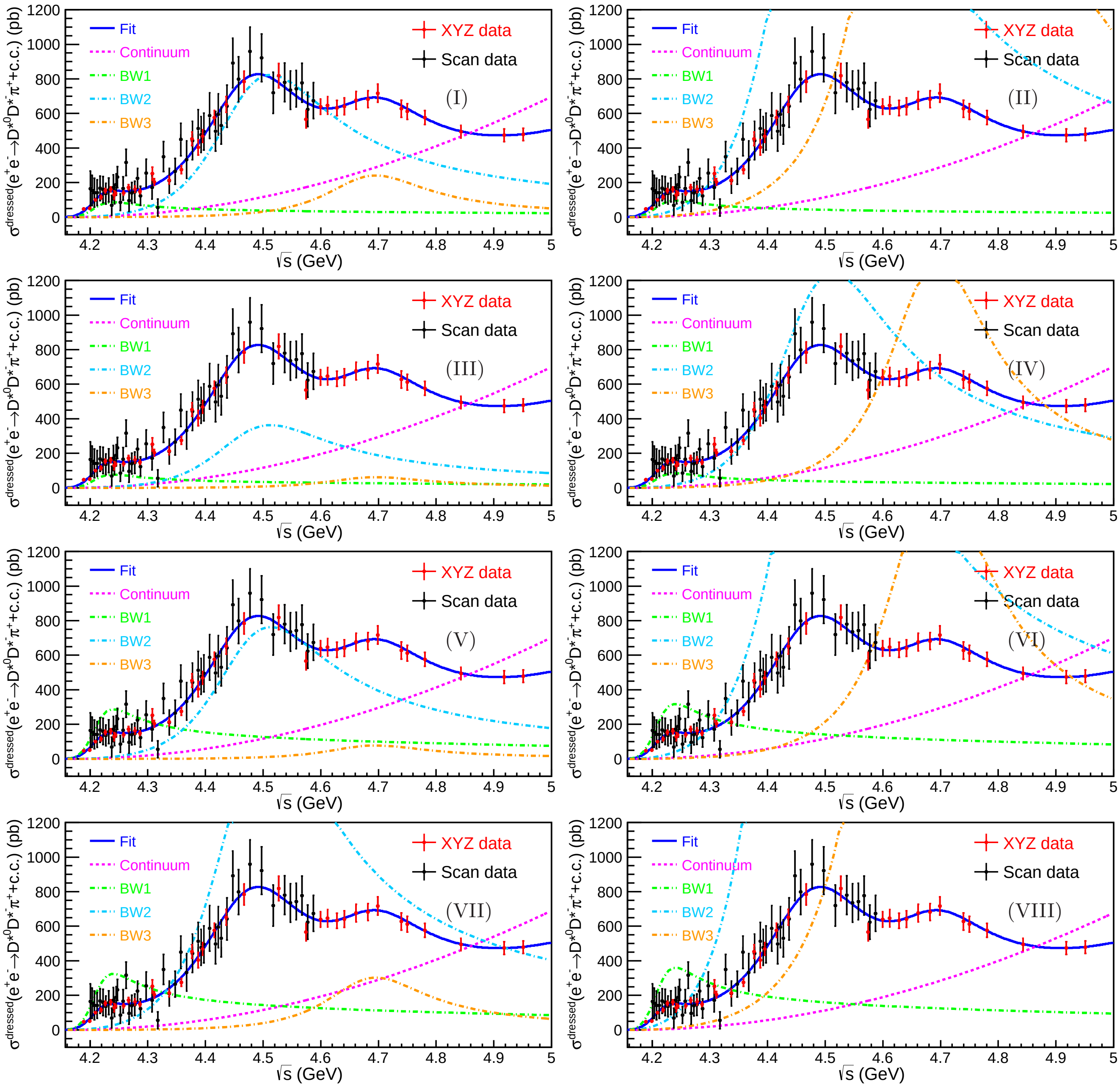

FIG. 2. The fit results of the dressed cross section line-shape of $e^+e^- \to D^{*0}D^{*-}\pi^+ + c.c.$. The blue curve is the total fit. The green, azure and orange dashed curves describe three BW functions, and the pink dashed-curve is the three body phase space contribution.

Appendix D: Systematic uncertainties

The systematic uncertainty studies are performed at energy points where the signal yield greater than 500 events. For other points suffering limited statistics, the uncertainty from the closest point is taken as its systematic uncertainty. All the systematic uncertainties are studied on each tag method separately and then combined together according to their yields. To consider all the related systematic uncertainties in the measurement of the Born cross sections, the sources of systematic uncertainty are divided into three categories.

The first category includes uncertainties associated with the detection efficiencies, such as tracking, particle identification, π^0 reconstruction, signal region requirements of the reconstructed unstable particles (*i.e.*, the $P^*(\pi^0)$ momentum rejection region, $D^0(D^-)$ and $D^{*0}(D^{*-})$ mass window requirements), MC simulation model and ISR correction factors. The uncertainty of detection and PID efficiency is 1.0% for each charged track [53], and 2.0% for π^0 reconstruction [54]. The uncertainties associated with the $P^*(\pi^0)$, $M(D^0(D^-))$ and $M(D^{*0}(D^{*-}))$ windows are estimated by re-extracting the detection efficiencies with Gaussian-smeared MC samples where the Gaussian parameters are obtained from the discrepancies between data and MC simulation. The MC samples are corrected according to the partial-wave-analysis (PWA) results at each energy points. To estimate the uncertainties from PWA-corrected MC samples, the samples with different PWA results are re-corrected by changing the possible components used in the PWA. The differences of efficiencies extracted from nominal and re-corrected MC samples are taken as the systematic uncertainty of the signal model. The ISR correction factors can have an impact on the detection efficiencies by affecting the slope of the line-shape and can be treated together, as $(1+\delta^{\rm ISR})\cdot\epsilon$, to estimate the uncertainty from ISR correction. Since the ISR correction factors are estimated by the fitting-iteration method, the uncertainty of this item comes from four different parts: the differences between the last two iterations are taken as the uncertainty of the iteration method itself; the uncertainty from the line-shape fitting model used in the iteration are estimated by replacing the PHSP model with a parameterized function; the uncertainty of $(1+\delta^{\rm ISR})\cdot\epsilon$ is estimated by 500 groups of cross-section toys which are re-sampled according to the uncertainty of the parameters and the corresponding covariance matrix; the vacuum polarization factors are taken from QED calculation at each energy point and affect the slope of the line-shape, its uncertainty is estimated to be 0.5%.

The second category includes uncertainties associated with the signal shape, background shape and fit range, which affect the estimation of signal yields. The uncertainty of the signal shape is estimated by convolving it with a double-Gaussian function in the fit instead of a single Gaussian function in the nominal results. The description of background shape is changed from a 2$^{\rm nd}$ order Chebyshev function to a linear function in the fit and the differences between the two cases are considered as the uncertainty. The uncertainty associated with the fit range is determined by altering the fit range from $(1.91, 2.12)\,{\rm GeV}/c^2$ to $(1.911, 2.12)\,{\rm GeV}/c^2$.

The last category includes the luminosity, quoted BFs where the uncertainty in luminosity is 1.0% at each energy point [46–48], and the uncertainty from quoted BFs of intermediate states in the subsequent decays, which are taken from the PDG [1].

Assuming no significant correlations between sources, the total systematic uncertainty is obtained as the sum in quadrature. Table III summarizes the systematic uncertainties of the cross section at various energy points.

TABLE III. The summary of all the systematic uncertainties in the Born cross section measurement. The items marked with '†' are treated as fully correlated uncertainties, the others are uncorrelated uncertainties. (unit: %)

$\sqrt{s}$ (GeV)	Track†	PID†	$\pi^{0\dagger}$	Signal region	Decay Model	$(1+\delta^{\rm ISR})^\dagger$	Signal shape	Bkg. shape	Fit range	$\mathcal{L}_{\rm int}^\dagger$	$\mathcal{B}^\dagger$	Total
4.226	3.7	3.7	2.8	0.5	0.9	1.4	2.5	0.9	3.1	1.0	2.7	7.9
4.236	3.7	3.7	2.7	0.4	0.3	1.0	2.3	0.5	2.6	1.0	2.7	7.6
4.244	3.6	3.6	2.8	0.6	0.6	0.8	1.0	1.2	1.3	1.0	2.7	6.9
4.258	3.6	3.6	2.8	0.6	0.0	0.7	2.6	2.5	3.2	1.0	2.7	8.1
4.267	3.6	3.6	2.8	0.7	0.1	0.7	1.8	0.5	1.8	1.0	2.7	7.1
4.288	3.7	3.7	2.8	0.2	0.1	1.9	1.6	1.6	1.6	1.0	2.7	7.3
4.312	3.6	3.6	2.7	0.3	0.6	2.9	1.6	3.0	1.5	1.0	2.6	8.0
4.337	3.6	3.6	2.7	0.4	0.5	2.3	1.9	6.0	2.1	1.0	2.7	9.6
4.358	3.7	3.7	2.8	0.5	0.1	2.3	1.3	2.5	1.7	1.0	2.7	7.7
4.377	3.7	3.7	2.7	0.4	0.4	1.2	0.9	4.6	1.7	1.0	2.7	8.3
4.397	3.7	3.7	2.8	0.3	0.6	0.6	0.9	2.7	0.8	1.0	2.7	7.3
4.416	3.7	3.7	2.7	0.6	0.4	0.8	0.2	2.3	0.5	1.0	2.7	7.0
4.436	3.7	3.7	2.8	0.3	0.2	0.9	1.2	1.3	0.0	1.0	2.7	6.8
4.467	3.7	3.7	2.7	0.5	0.6	1.0	0.3	1.5	0.4	1.0	2.7	6.8
4.527	3.7	3.7	2.7	0.4	0.4	0.9	3.1	1.0	2.5	1.0	2.7	7.8
4.575	3.7	3.7	2.8	0.5	0.3	0.6	1.1	0.6	0.4	1.0	2.7	6.8
4.600	3.7	3.7	2.7	0.5	1.2	0.9	0.5	0.3	0.7	1.0	2.6	6.8
4.612	3.7	3.7	2.8	0.2	0.4	1.1	0.5	0.7	0.5	1.0	2.7	6.7
4.628	3.7	3.7	2.7	0.4	0.1	1.3	0.7	0.9	0.4	1.0	2.6	6.8
4.641	3.7	3.7	2.7	0.3	1.0	2.7	0.7	1.1	0.8	1.0	2.7	7.3
4.661	3.7	3.7	2.8	0.3	2.0	2.6	0.6	0.3	0.1	1.0	2.7	7.3
4.681	3.7	3.7	2.7	0.3	0.5	2.4	0.2	0.5	0.1	1.0	2.7	7.0
4.698	3.7	3.7	2.7	0.2	1.0	2.5	0.1	1.1	0.4	1.0	2.7	7.2
4.740	3.7	3.7	2.7	0.5	2.5	1.5	0.5	0.8	0.8	1.0	2.6	7.3
4.750	3.7	3.7	2.7	0.3	2.1	1.0	0.1	0.6	0.5	1.0	2.6	7.0
4.781	3.7	3.7	2.7	0.4	0.4	0.8	0.2	0.4	0.9	1.0	2.6	6.7
4.843	3.7	3.7	2.7	0.2	2.1	1.2	0.4	0.9	0.6	1.0	2.6	7.1
4.918	3.7	3.7	2.7	0.4	1.8	1.2	0.4	1.4	0.5	1.0	2.6	7.1
4.951	3.7	3.7	2.8	0.4	0.6	0.8	0.6	1.6	0.6	1.0	2.7	6.9